Journal of CO2 Utilization 53 (2021) 101749

Contents lists available at ScienceDirect

Journal of CO2 Utilization

journal homepage: www.elsevier.com/locate/jcou

Electrocatalytic conversion of CO_2 over in-situ grown Cu microstructures on Cu and Zn foils

Anchu Ashok [a], Anand Kumar [a,*], Mohammed Ali Saleh Saad [a,b], Mohammed J. Al-Marri [a]

[a] Department of Chemical Engineering, College of Engineering, Qatar University, Doha, P O Box 2713, Qatar
[b] Gas Processing Center, College of Engineering, Qatar University, Doha, P O Box 2713, Qatar

ARTICLE INFO

Keywords:
CO_2 reduction
Electrocatalysis
Formic acid
Shape-controlled synthesis

ABSTRACT

Electrochemical conversion of carbon dioxide to value added multi-carbon products is of great importance and a promising approach to mitigate greenhouse gases. In this work, we report the fabrication of electrodes by depositing Cu over the metallic foils of Cu and Zn, which show high faradic efficiency for the conversion of CO_2 to formic acid, acetate, and methanol. The morphology, phase and oxidation state of the Cu were different on the two foils while maintaining the same synthesis steps. The Cu particles embedded on Cu foil (Cu/Cu-foil) are in 3D cuboids form with flat and smooth faces, whereas Cu on Zn foil (Cu/Zn-foil) emerge in the shape of 3D flowers with the club of Cu microspikes grown perpendicularly from a root. For the electrocatalytic conversion of CO_2, the Cu/Cu-foil shows a high selectivity for formic acid and ethyl acetate with the highest faradaic efficiency of 78 % at −0.3 V vs RHE, and 64 % at −1.0 V (vs RHE) for the two products, respectively. In contrast, the Cu/Zn-foil displays a high selectivity towards methanol, with the highest faradaic efficiency of 48 % at −1.0 V vs RHE, indicating that the product selectivity can be easily modulated by changing the metallic foil on which the Cu particles are deposited. Both the electrodes, Cu/Cu-foil and Cu/Zn-foil, show long-term stable performance while maintaining the selectivity of the products during CO_2 electrocatalytic conversion.

1. Introduction

Currently, fossil fuels meet ~ 80 % of total energy requirement for human beings owing to a higher current density than other energy systems that has adversely affected the environment by increasing the CO_2 emissions resulting in severe environmental challenges, as CO_2 is considered to be one of the major contributors to global warming [1–4]. On the other hand, CO_2 is also an essential material for the growth of vegetation and many industrial processes. In order to maintain the ecosystem stability, in an ideal scenario, the total release of CO_2 in the environment from all the sources should be balanced with the amount being consumed. Considering the worldwide total energy consumption trends, it is challenging to stop using fossil fuels until developing and adopting environmentally clean energy systems. Another possible approach is to capture and sequestrate CO_2 geologically or to convert CO_2 into useful chemicals such as low-carbon fuels and commodity compounds. Simultaneous efforts are underway in both the directions, as green energy technologies based on environmentally friendly energy resource such as solar, wind, tidal and biomass energies are growing rapidly; whereas many research groups are attempting to convert the atmospheric CO_2 into useful chemicals such as formaldehyde, formic acid, alcohols, methane, and CO via thermal, photo- or electro-catalytic routes [5–11].

CO_2 molecules are fully oxidized and thermodynamically stable and its conversion to reduced carbon species through electrolysis in aqueous medium is challenging due to the poor kinetics [12–14]. The conversion of CO_2 into value added chemicals using different approaches such as photochemical, thermochemical and electrochemical methods is yet to commercialize [15,16]. Out of these methods, more attention was paid in the development of electrochemical mode of CO_2 conversion owing to the attractive features and advantageous when compared to other methods [17,18]. The electrochemical CO_2 reduction offers the opportunity to conduct the reaction at ambient condition and tune the rate of reaction through the external bias i.e. overpotential. Moreover, the electrocatalyst selectively produce the desired products and suppress the undesired side reaction to improve the efficiency of the system for the production of value-added products from CO_2 as fuel source. The majority of existing electrocatalysts fall under the category of mono-metallics, bimetallics, non-metallics, ion modified-metallics and molecular catalysts that provides wide opportunities for CO_2

* Corresponding author.
E-mail address: akumar@qu.edu.qa (A. Kumar).

https://doi.org/10.1016/j.jcou.2021.101749
Received 30 July 2021; Received in revised form 26 September 2021; Accepted 2 October 2021
Available online 7 October 2021

electroreduction [16,19–23]. Based on the product formed during CO_2 reduction the electrocatalyst can be categorized as; hydrogen selective (e.g., Pt, Fe, Ni), formate selective (e.g., Sn, In, Pb) and CO selective (e.g., Ag, Au, Zn) [24–32]. Copper based catalysts, on the other hand, have shown the potential to synthesize a wide variety of value added chemicals including CO, ethylene, formate, methane, alcohols, and acetate simultaneously; though with varying selectivity [16,33,34]. However, copper catalysts are also reported to be highly vulnerable to poisoning and deactivate quickly, in many cases in less than an hour [35,36]. To overcome this challenge, many research groups are now focusing on the strengthening structural properties to enhance the selectivity and stability of the Cu based catalysts. Metal-organic framework (MOF) are another class of crystalline materials with uniform pores and regular frame structure made up by coordinating bridging organic ligands with metal centers that exhibit promising ability for electrocatalytic CO_2 reduction. MOF exhibits excellent physio-chemical properties such as excellent conductivity, high surface area, improved pore size, controllable morphology and tunability, more accessible active sites that enhances the CO_2 conversion. Monoatomic dispersion achieved through the metal-ligand periodic interval in MOF promotes the adsorption and allows to have more accessible active sites in MOF. To date, CO_2 electroreduction has been reported to be catalyzed by various MOF derived pristine materials, MOF on supports, MOF encapsulated with metal/-metal oxide particles, and MOF derived single atom catalysts. Zhao et al. conducted an extensive review of utilizing MOF based materials as effective approach for electrochemical CO_2 reduction reaction [37]. In recent years, researchers put great effort on developing a new classification of 2D transition metal nitride/carbide materials named as MXene that can be developed via etching of MAX phase where M is the transition metal phase, A be the main group sp element and X be C or N atoms [38]. The catalytic active sites of MXene originate from the enormous metallic atoms containing empty d-orbitals that enhances the gas adsorption and the intrinsic properties of metal that enhances the electron transfer. Li and co-workers provided a theoretical analysis on using MXene M_3C_2 materials for the electrochemical conversion of CO_2 to CH_4. The DFT analysis shows a better understanding of the active sites and the expected pathway of CH_4 formation over MXene catalyst [39].

In this work, our objective is to develop self-supported copper electrocatalysts directly grown on rigid materials like metallic foils without any binders or additives. The self-supported electrocatalyst possesses large electrochemical active surface area with easy electrolyte penetration that enable facile access of reactants to active sites. A 3D porous architecture allows an effective charge transfer between the electroactive species and the substrate. The direct growth of the active material on the metal foils avoid the weak contact between the particle and support and offers a strong adhesion of particle and the support to prevent the falling off of the active material from the substrate resulting in an enhancement in the stability of the electrode. Moreover, these self-standing materials improve the electrochemical properties of the catalyst through the tailoring of the morphology and tuning the active phase of the materials on the support. These designs with high activity and stability are very much suitable for large-scale applications that can pave a way to commercialization. Moreover, in this work we studied the effect of metal support on CO_2 conversion to find how the support affects the selectivity of the product molecules.

2. Synthesis procedure

All the chemicals and materials were purchased from commercial companies and used without any further treatments. Before synthesizing the particles, the bare Cu and Zn foils were washed by sonicating them in acetone, ethanol, and DI water respectively for 30 min; and dried at 70 °C for 3 h. In a typical process, 1 mmol copper nitrate $Cu(NO_3)_2{\cdot}3H_2O$, 2 mmol urea ($CO(NH_2)_2$) are added to a given amount (75 mL) of distilled water and dispersed to form a homogeneous solution by constant stirring. Thereafter a 3 mL of 0.1 M NaOH was added dropwise, and the solution was continuously stirred for another 15 min. After putting a piece of cleaned copper foil, the solution was then transferred into a Teflon-lined stainless steel autoclave reactor. The autoclave was sealed and maintained at 120 °C for 15 h, thereafter it was removed from the furnace to cool down the temperature. Once the reactor the reactor is cool enough, the product was collected, washed, dried at 60 °C for 2 h to remove the excess residuals from the surface. It was further dried at 60 °C for 3 h in open air to remove the water content. Fig. 1 shows the schematic representation of the hydrothermal synthesis process for the synthesis of Cu/Cu-foil and the real images of the bare Cu foil and the Cu foil loaded with Cu nanoparticles are shown in Fig. S1". The procedure for Cu/Zn-foil is similar as above, except Zn foil was as a support to deposit the Cu microparticles.

3. Material characterization

The crystallinity of the particles was measured using PANalytical Empyrean XRD unit with a scan range of 10−90 ° at 0.154 nm wavelength of Cu-Kα radiation source. Nova Nano 450 FEI scanning electron microscope (SEM) coupled with the EDX unit within the magnification of 200 kx was used to identify the morphology of the particle synthesized. X-ray photoelectron spectroscopy, XPS, Kratos AXIS Ultra DLD was used to identify the oxidation state, bonding configuration, and chemical composition of the synthesized particles on the surface.

4. Electrochemical measurement

Zahner electrochemical workstation along with a customized three cell electrode system with 0.1 M $KHCO_3$ electrolyte was used to evaluate the electrochemical CO_2 conversion of the catalysts. Particle deposited metal foil (Cu/M-foil, M = Cu, Zn) were used as the working electrode, Ag/AgCl (4 M KCl) as the reference electrode and a carbon cloth was used as the counter electrode. The working electrode was electrochemically pre-treated with a scan rate of 500 mV s^{-1} for 50 cycles in the potential range from −2 to 0.4 V with N_2 and CO_2 saturated 0.1 M $KHCO_3$ electrolyte to remove any unwanted residues. Cyclic voltammogram was conducted in the potential window of -1.4 to 1.0 V vs RHE at a scan rate of 50 mVs^{-1} in N_2 and CO_2 saturated electrolytes to understand the CO_2 conversion profile. Chronoamperometry (CA) was conducted to perform the stability test of CO_2 reduction at different potentials under CO_2 saturated electrolyte for 30 min, and the liquid electrolyte was collected for product identification. The dissolved products in electrolyte after CA were measured using a high-performance liquid chromatography (HPLC, WATERS Acquity UPLC) coupled with Column Acquity UPLC BEH C18 1.7um, 2.1 × 50 mm. A 1 mM $HClO_4$ at 0.2 mL/min mobile phase and a UV detector at 210 nm were used for analysing the products. Analysis of low boiling point liquids (e.g. methanol, formic acid etc.) were also conducted using a gas chromatograph (PerkinElmer, Clarus 680) equipped with FID detector at 320 °C with Air and H_2 gas flow of 450 and 45 mL/min respectively, using He as a carrier gas at 1 sccm. All the potential measured against standard reference electrode is converted to reverse hydrogen electrode (RHE) using the equation E (versus RHE) = E (versus Ag/AgCl) + 0.199 V + 0.0591 x $pH_{electrolyte}$.

5. Results and discussion

Fig. 2a shows the XRD profile of the Cu particles deposited over Cu foil (Cu/Cu-foil) and Zn foils (Cu/Zn-foil). The XRD of Cu particles are uniformly grown over Cu foil confirm the existence of Cu_2O (98-005-375 7) and metallic Cu (98-005-204 3) phases. Reduction route of Cu^{2+} depends on various factors including the temperature, pH and the type of the reducing agent used. Chen and Xue reported a chemical reaction controlled crystallization of Cu_2O particles with shape evolution from nanowires to truncated octahedra and cubohedra structure through a two-step "precursor formation crystallization" process [40]. They

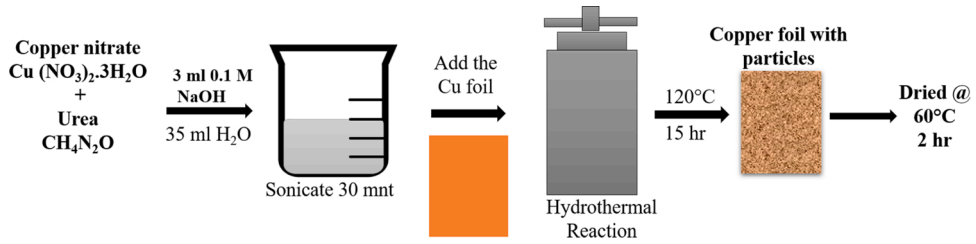

Fig. 1. Schematic representation of the hydrothermal synthesis of Cu/Cu foil.

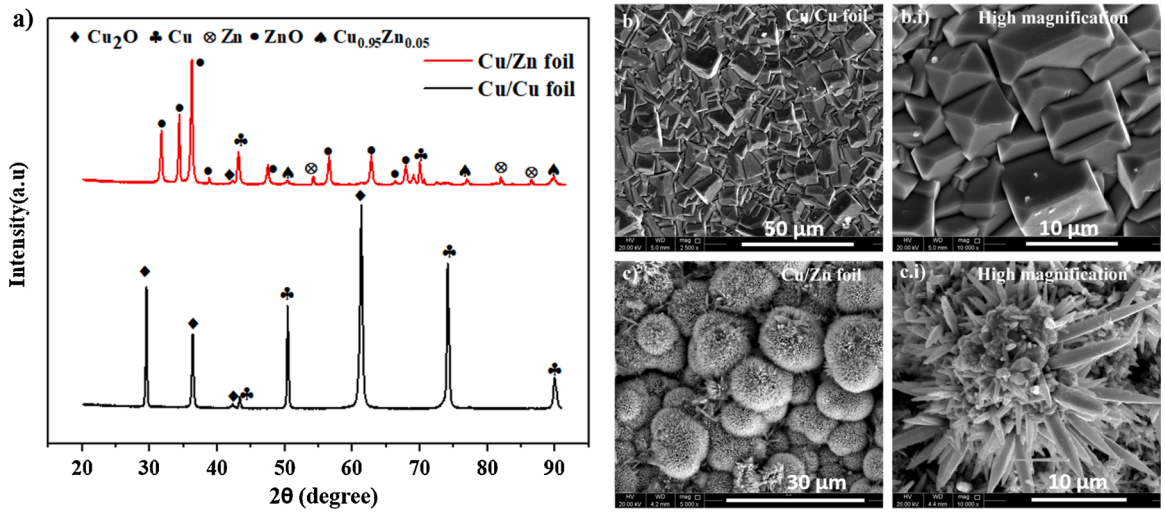

Fig. 2. a) XRD profile of Cu/Cu-foil and Cu/Zn-foil. SEM micrograph of Cu/Cu-foil: b) low magnification), b.i) high magnification; and Cu/Zn-foil: c) low magnification, c.i) high magnification.

studied the effect of adding a slight amount of OH^- ion into initial precursor solution that controlled the crystallization of Cu_2O/Cu. The composition of the product depends on the ratio of OH^-/Cu^{2+}. At higher OH^- concentration, the reaction favors the formation of CuO crystals and the mechanism of redox system is as follows

$$Cu^{2+} + 2OH^- \rightarrow Cu(OH)_2 \quad (1)$$

$$Cu(OH)_2 + 2OH^- \rightarrow Cu(OH)_4^{2-} \quad (2)$$

$$2Cu^{2+} + 3OH^- + NO_3^- \rightarrow Cu_2(OH)_3NO_3 \quad (3)$$

The size of the particles formed can be selectively tuned with the pH and the control of pH-dependent chemical reaction is an effective way to define the crystallization of particles.

The crystallinity of Cu particles changed when Zn foil is used instead of Cu foil. During the reduction of Cu^{2+} precursors in presence of Zn foil, a chemical attachment of Cu microparticle with Zn is confirmed by the presence of $Cu_{0.95}Zn_{0.05}$ phase in the XRD. Copper microstructure further grows on the $Cu_{0.95}Zn_{0.05}$ phase, and the XRD further confirms the formation of ZnO (along with Zn) from Zn foil. The SEM result in Fig. 2b show the presence of 3D cuboids of Cu particles on the Cu foil, with the high magnification image indicating the existence of cuboid structures with flat smooth faces in the size range of 2–5 µm. The EDX spectrum (Fig. S2) shows the presence of Cu on the surface of the catalysts. The micrograph of Cu/Zn-foil in Fig. 2c shows the presence of a thickly grown flower like structure (low magnification), in which each flower is made up of Cu microspikes grown perpendicularly from a shared root (high magnification). The EDX spectrum shows the presence of Cu and Zn in almost 1:1 ratio (Fig. S2).

The electrochemical behavior of the electrodes were further evaluated using cyclic voltammogram of Cu/Cu-foil and Cu/Zn-foil in N_2 and CO_2 saturated 0.1 M $KHCO_3$ electrolyte. The voltammogram profile in Fig. 3 shows an increase in the current density after CO_2 saturation that clearly demonstrates the ability of catalysts towards CO_2 electrochemical reduction. At -1.4 V vs RHE, the current density of Cu/Cu-foil is -18 $mAcm^{-2}$ and for Cu/Zn-foil the value increased to -30 $mAcm^{-2}$ confirms the higher activity of Cu particles deposited over the Zn foil. The synergetic effect of Cu and Zn significantly tune the activity and selectivity of the CO_2 conversion. Chronoamperometric analysis of electrodes under CO_2 saturated 0.1 M $KHCO_3$ is shown in Fig. 3b (Cu/Cu-foil) and 3d (Cu/Zn-foil) shows a stable current profile at wide range of potential between -0.3 V to -1.9 V vs RHE. There is an increase in the current value at higher potentials, which may be associated with a high conversion of CO_2 into products. In addition, a high current density if consistently maintained to confirm the electrochemical stability of the catalysts.

Fig. 4 shows the faradaic efficiency of the products identified after the chronoamperometric analysis conducted at different potentials. The result shows that Cu/Cu-foil is more selective to formate and acetate where the formate shows the highest faradaic efficiency of 78 % at -0.3 V vs RHE and decreases the efficiency with an increase in the potentials. The faradaic efficiency of acetate in presence of Cu/Cu-foils hold the highest value of 64 % at -1.0 V vs RHE and dropped drastically beyond this potential value. Grosse et al. demonstrated an interesting correlation between the Cu nanocubes and the support, and they found that Cu cubes on Cu foil is more selective to C_2-C_3 products, meanwhile Cu cubes on carbon foil is selective to C_1 products only. It was clear that, higher C_2/C_1 product ratio was observed for Cu over Cu foil as compared to Cu cubes supported in C [41]. The analysis of the products in Cu/Zn-foil shows the existence of formate and methanol as products in the electrolyte. The presence of formic acid is at the highest value of 28 % at −0.3 V vs RHE and methanol hold a value of 48 % at −1.0 V vs RHE. The results show that Cu/Zn-foil is more selective to methanol and less

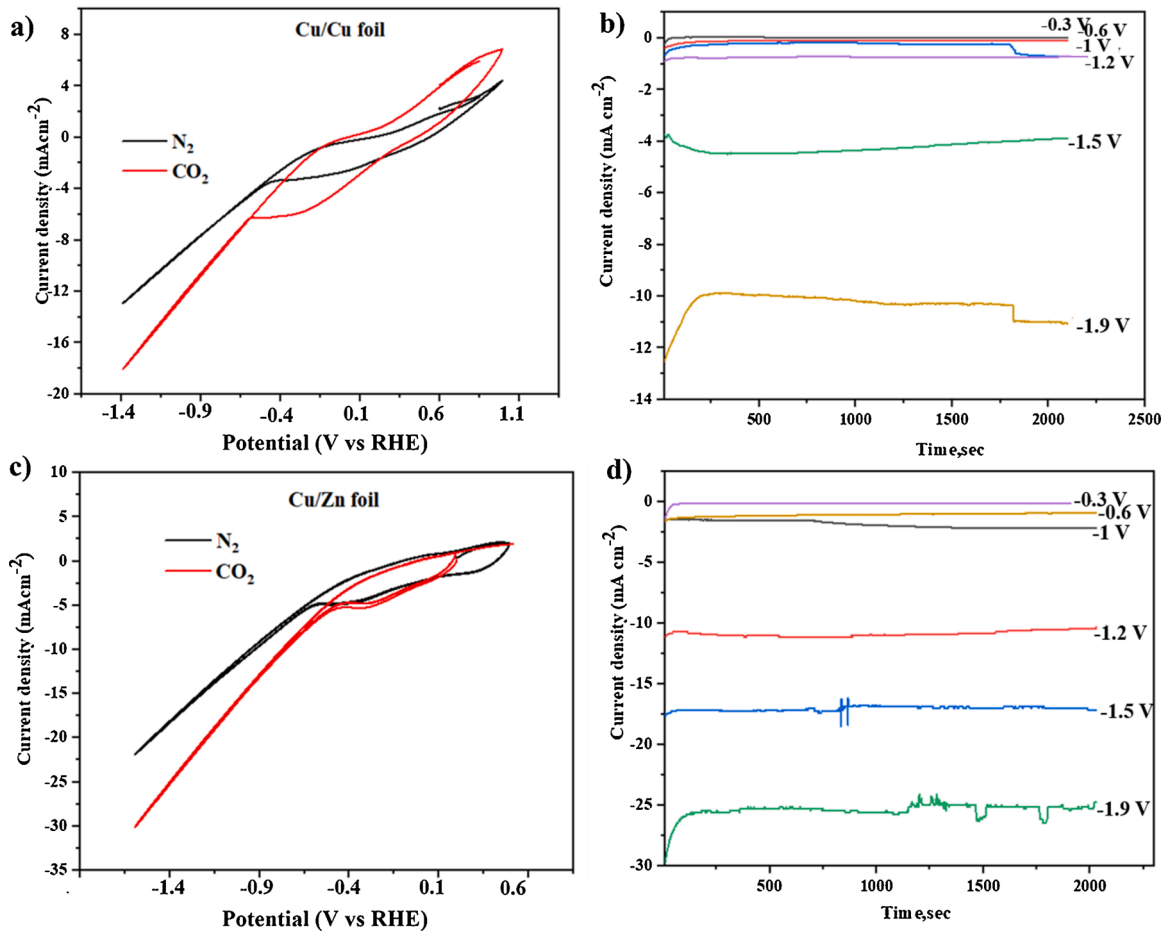

Fig. 3. Cyclic voltammograms (CV) of a) Cu/Cu foil c) Cu/Zn foil in N_2 and CO_2 saturated 0.1 M $KHCO_3$ solution. Chronoamperometric analysis of b) Cu/Cu foil d) Cu/Zn foil at different potential for product identification.

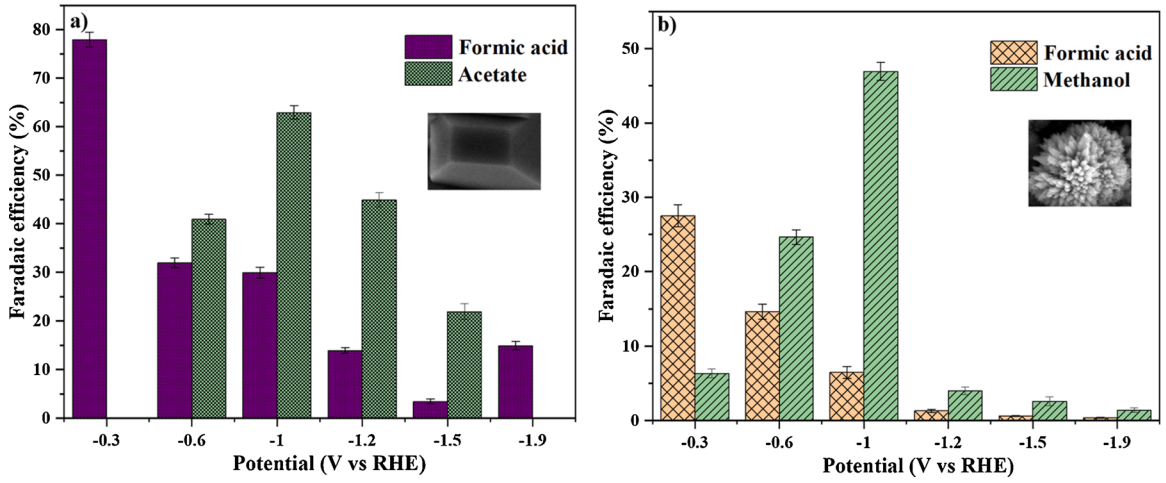

Fig. 4. Faradaic efficiencies of the products identified in a) Cu/Cu foil and b) Cu/Zn foil electrode in CO_2 saturated 0.1 M $KHCO_3$ solution.

selective to formic acid when compared to Cu/Cu-foil.

Methanol formation through the CO_2 electrochemical conversion can be achieved via two reaction pathways. CO_2 can be converted to methanol through a CO intermediate pathway, or through the formation of a formate ion as an intermediate [42]. The presence of formic acid indicates the formation of methanol through the latter pathway as shown below.

$$CO_2 + e^- + H^+ = HCOO\text{-} \text{ (Formate ion)} \quad (4)$$

$$HCOO^- + e^- + H^+ = HCOOH \text{ (Formic acid)} \quad (5)$$

$$HCOOH + e^- + H^+ = HCO + H_2O \quad (6)$$

$$HCO + e^- + H^+ = CH_2O \text{ (Formaldehyde)} \quad (7)$$

$$CH_2O \text{ (Formaldehyde)} + 2e^- + 2H^+ = CH_3OH \text{ (Methanol)} \quad (8)$$

Overall reaction: $CO_2 + 6e^- + 6H^+ = CH_3OH + H_2O$ (9)

The conversion of CO_2 to CH_3OH through the 6-electron pathway is kinetically slower and needs highly active catalysts to overcome the energy barriers. Lan and co-workers conducted a study on the electrochemical performance of Cu(core)/Cu(shell) and developed a model that followed a first-order reaction of CO_2 to CO and HCOOH [43]. The model describes the formation of HCOOH and CO could be helpful on the further formation of CH_3OH on the Cu based catalyst materials. The same group conducted experimental study on Cu(core)/Cu(shell) catalyst in a flow reactor and confirmed the presence of CO, HCOOH and CH_3OH as the main products. Kyriacou et al. studied the acceleration of electrochemical reduction of CO_2 into CH_3OH on Cu-Sn-Pb based alloy by varying the cations and changing the composition of the electrolyte. The main products formed during the electroreduction was CH_3OH, CO and HCOOH [44]. Andrew and team used Cu electrode and Cu nanoclusters on single crystal ZnO electrode to generate CH_3OH, CH_3CH_2OH, HCOO, methyl formate and traces of C_3H_8O. The faradaic efficiency of formate on Cu(111) was found to be 11.8 % and on Cu/ZnO the value reduced to 7.7 %. They proposed the use of ZnO as an electrocatalyst to strengthen the selectivity towards alcohols. Formation of methanol on Cu/Zn-foil is a clear indication that Cu/Zn-foil is a promising catalyst for effectively synthesizing methanol from CO_2 [45]. Albo et al. conducted a similar study on Cu_2O/ZnO surface towards the electrochemical synthesis of methanol from CO_2 reduction with the highest faradaic efficiency of 17.7 % [46]. The current study provides an option to further improve the Cu/Zn catalyst with a superior faradaic efficiency of 48 % and excellent long-term stability. It is worth noting that in this work, compared to the previous literature, the alcohol selectivity increases manifold with the use of Cu/Zn electrode relative to bare Cu (111) surface. The nature of this trend in selectivity is not clear;

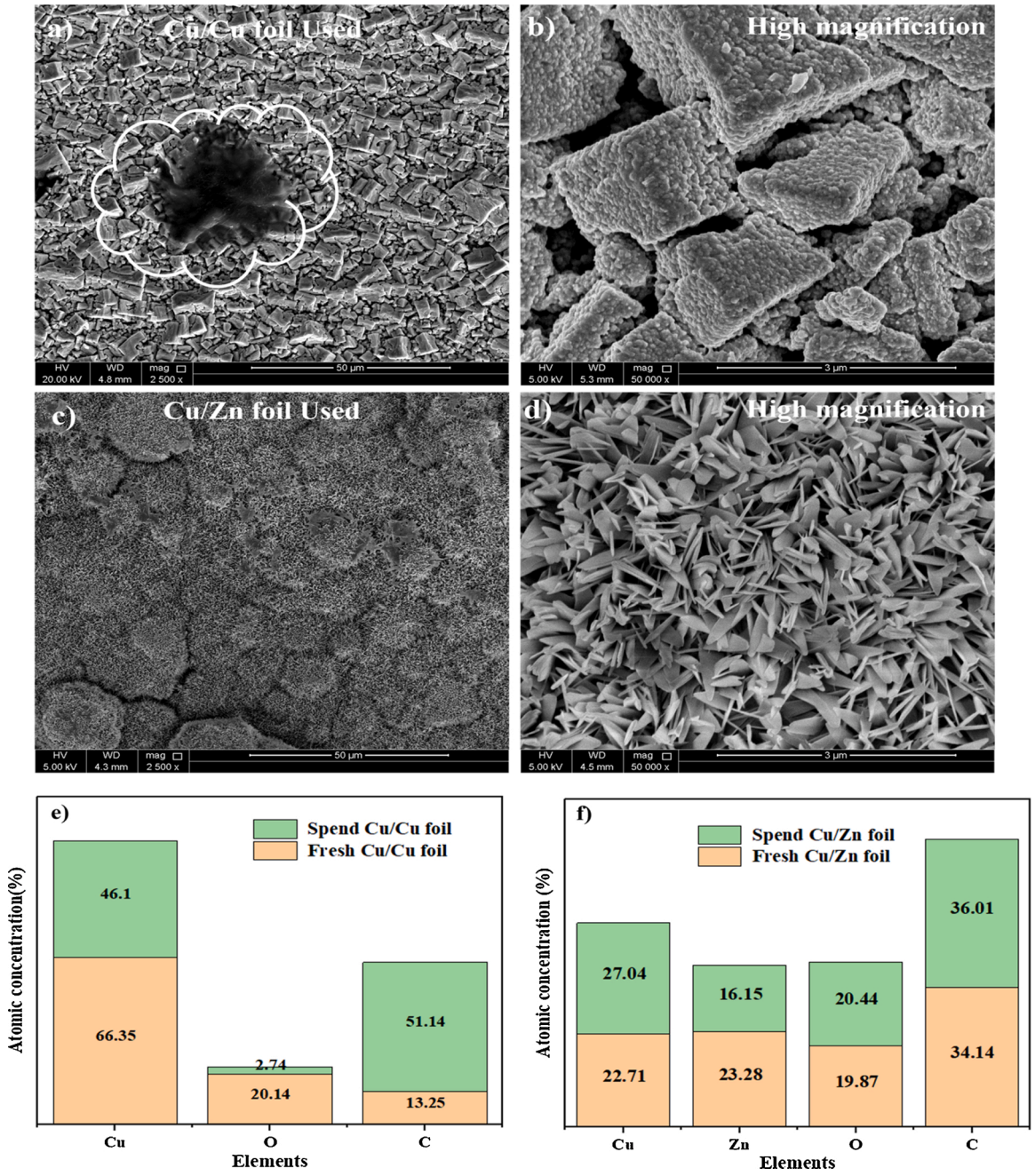

Fig. 5. SEM micrograph of spend Cu/Cu-foil a) low magnification b) high magnification synthesized; and Cu/Zn foil c) low magnification d) high magnification synthesized. Elemental analysis on the fresh and spend catalyst of e) Cu/Cu foil f) Cu/Zn foil.

however, there are some possible mechanism that can be proposed. The C_2-alcohol products selectivity are considered as the function of the electrode surface and the co-ordination level of Cu surface. The ZnO particles supports low-coordinated Cu sites that favor the formation of alcohols. Another impact is the interaction between the Zn and Cu sites on the catalyst surface that forms a "Cu-ZnO synergy" effect as reported elsewhere [47]. The DFT calculation on the gas-phase synthesis reaction shows that the Cu-Zn interactions influence the reduction pathway and suggests that Zn plays a direct role in the activation of the reactants that form methanol at the Cu sites with Zn atoms at stepped surface, which strengthen the binding of the intermediate species and allow the reaction to proceed further. In addition, it is evident that the Cu atoms near the ZnO develop a positive charge that is beneficial for the absorption of CH_3O adsorbates. Moreover, Cu has the ability to break C—O bond and proceeds with the addition of hydrogen to form C—H bonds, whereas the presence of Zn helps in the adsorption of OH group. This synergy establishes Cu and Zn as excellent choices for methanol synthesis from synthetic gas. The formyl adsorbate attracts the protons from the nearby OH group to form formaldehyde then converts to methoxy species upon the addition of hydrogen. Several spectroscopic studies with bond vibrational analysis such as Thermal Desorption Spectroscopy (TDS) and High-Resolution Electron Energy Loss Spectroscopy (HREELS) identified the presence of stretching O—H bond on ZnO surface that indicates the formation of OH species upon the exposure of ZnO to water at room temperature. The adsorption OH group on the electrode surface is a key step towards methanol synthesis and the presence of OH binding sites improves the methanol selectivity. While using Cu-Zn interface electrodes, Cu improves the electrode conductivity and Zn provides more adsorption sites for OH by creating Cu—OZ—n stable and active sites for CO_2 electroreduction to methanol.

6. Analysis of spend catalyst after CO_2 reduction

The SEM micrograph of the particles supported metal foils after the chronoamperometric analysis are shown in Fig. 5. The smooth surface of the Cu particles before the reaction are changed into rough surfaces after the CO_2 reduction, which could be due to the multiple oxidation-reduction cycles during the pretreatment procedure that make the catalyst surface more active and stable. Grosse et al. reported the dynamic change in the structure, composition, chemical state, and selectivity on Cu nanocubes deposited over carbon paper. They found that the original flat facet gets roughened in course of the reaction and results with porous nanocube with loss of sharp edges and corners [41]. The porous structure could have resulted from the progressive reduction of copper oxide into metallic form. During reaction, these pores and the cubic edges are more disposed to to the electrolyte than the flat facets and trigger the electrochemical reaction.

The emphasized region in Fig. 5a indicates the existence of carbon deposited on the surface of the catalyst. This is also evident from the EDX elemental composition that indicates an increase in carbon on the catalyst surface after the reaction, with carbon content being around 51.14 % after the reaction as compared to only 13.25 % on the fresh catalyst. The excess amount of carbon could be due to the deposition of some carbonaceous product after CO_2 reduction. There is also a significant reduction in the oxygen level on the surface of the catalyst due to the reduction of the catalyst surface during the reaction. The SEM images of Cu/Zn-foil show the transition of microspikes arrays into microplate structures of Cu over Zn foil after the electrochemical CO_2 reduction. Densely grown Cu particles over the metallic foil underwent a structural transformation to a more stable form during the period of CO_2 reduction. The morphological transition allows access of more active sites and enhances the reaction kinetics of CO_2 conversion. In Cu/Zn-foil, the amount of carbon increased about 2 % when compared to fresh Cu/Zn-foil. While comparing two catalysts, the carbon content is much higher in the Cu/Cu-foil electrode than the Cu/Zn-foil.

The XRD profiles before and after reaction in Fig. 6a shows the presence of mixed phases of Cu_2O and Cu before reaction, and some of the Cu_2O peaks are replaced by metallic Cu peaks after the electro-reduction reaction. This could be the reason for the reduction in oxygen content after the reaction as evident form EDX spectrum. Metallic Cu is a unique catalyst selective to higher electron transfer reactions favorable for the generation of bigger molecules of hydrocarbons and alcohols beyond the limit of two electron transfer products such as formates and CO. Previous reports show the instability of the sub-surface oxygen with more favorable oxygen position towards the surface than in the bulk position. Although, the stability of the oxygen is still questioned owing to the high electro-reductive nature of CO_2 reduction reaction [48], the transition of Cu_2O to metallic Cu phase promotes the selectivity of Cu particles to favor reactions with higher number of electron transfer. Swang and co-workers conducted a XANES analysis on the Cu based nanoparticles at -1.1 V RHE for 10 h electrolysis and found the metallic Cu to be the active site of catalyst [49]. The XRD profile of Cu/Zn-foil profile in Fig. 6b. shows the existence of Cu, Zn and CuZn on both fresh and used catalyst without much phase transition shows the stability of the catalyst, however there is a structural modification as discussed in previous section.

The fresh and used electrodes were further characterized using XPS analysis to understand the changes in electronic properties. The obtained binding energies of the XPS spectrum were corrected with respect to the C 1s spectrum (284.6 eV). The Cu 2p XPS spectrum of fresh and used samples is shown in Fig. 7a with two main peaks around 932 and 952 eV corresponding to the Cu $2p_{3/2}$ and Cu $2p_{1/2}$ spectrum

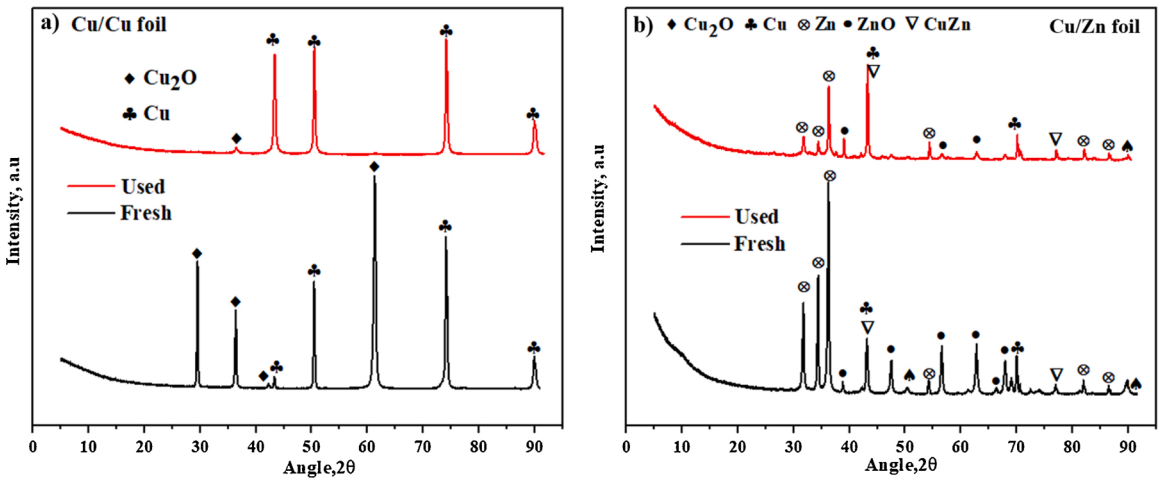

Fig. 6. Comparison of XRD profile of the fresh and used catalyst of a) Cu/Cu foil and b) Cu/Zn foil.

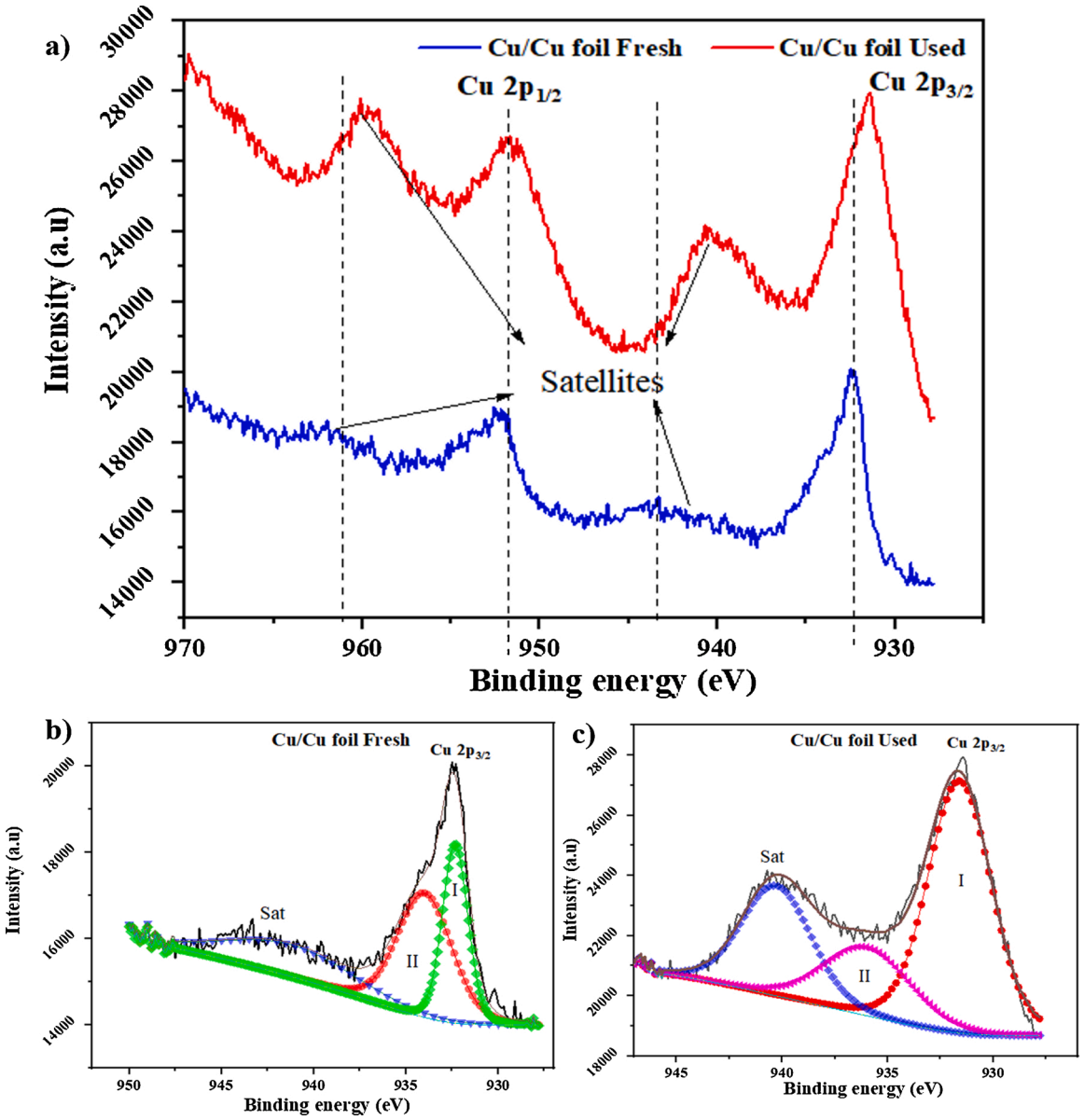

Fig. 7. a) XPS spectrum of Cu $2p_{3/2}$ for the fresh and used sample of Cu/Cu foil and the deconvolution spectrum of b) fresh Cu/Cu foil c) used Cu/Cu foil.

respectively along with the satellite peaks due to the shake-up of Cu^{+} electrons in the outer orbitals [50,51]. The shake-up peaks in used samples are stronger compared to the peaks corresponding to the fresh sample. The presence of weak satellite peaks in fresh catalyst confirm the existence of Cu_2O-Cu on the fresh sample and the strong peaks in used samples could be the presence of some traces of CuO that was not being detected by the XRD or the peaks were overlapping with the other phases of Cu in the XRD spectrum.

Fig. 7b-c shows the deconvolution spectrum of Cu $2p_{3/2}$ for Cu/Cu-foil fresh and used samples. In Cu/Cu-foil fresh catalyst, the major peak of Cu $2p_{3/2}$ at 932.3 eV confirm the presence of Cu(0) in the metallic form (Peak I) and the shoulder peak (Peak II) at 933.9 eV can be attributed to Cu (I) along with the weak satellite peak. The XPS results are consistent with the XRD analysis suggesting the existence of Cu and Cu_2O in the sample. While the peaks of Cu $2p_{3/2}$ in the used Cu/Cu-foil show the existence of the main peak at 931.6 eV corresponding to Cu(0), and a minor peak at 935.6 eV related to CuO along with the strong satellite peak [52]. A detailed analysis of deconvoluted O 1s spectrum is shown in Fig. 8. O1 s spectrum in Cu/Cu-foil consist of two unresolved peaks; one at 529.1 eV corresponding to O^{2-} species in Cu_2O phase, and another predominant peak at a higher binding energy at 531.4 eV attributed to the oxygen species adsorbed on the surface of the catalyst [53–57]. After the electroreduction, the peak of O^{2-} species disappeared and only the presence of absorbed oxygen existed. The high-resolution spectrum of C 1s in Cu/Cu-foil before and after electrochemical CO_2 reduction is shown in Fig. 8c-d. The deconvolution of C 1s spectrum in Cu/Cu-foil show the existence of three predominant peaks at 282.3 eV, 282.4 eV and 286.8 eV corresponding to the metal-carbon bond, C═C (sp^2 carbon) and C—OC— (epoxy carbon). During the synthesis process, the carbon atoms can get diffused into the atomic layer of Cu and generate Cu-C matrix. The deconvolution of C1 s spectrum in the foil after CO_2 electrochemical reduction consist of two main spectral regions. The first envelop at lower binding energies represents a considerable degree of oxidation with functional group and composing structures that includes the Cu—C bond, CC and CO═— at 282.0 eV, 283.5 eV and 285.6 eV respectively. Whereas, the second envelop at higher binding energies are assigned to the highly oxidized carbon species and physically/chemically adsorbed CO_2 or the intermediate species [58–61]. The deconvolution C1 s profile at higher binding energy consist of two broad peaks pointed at 289.7 eV and 292.34 eV

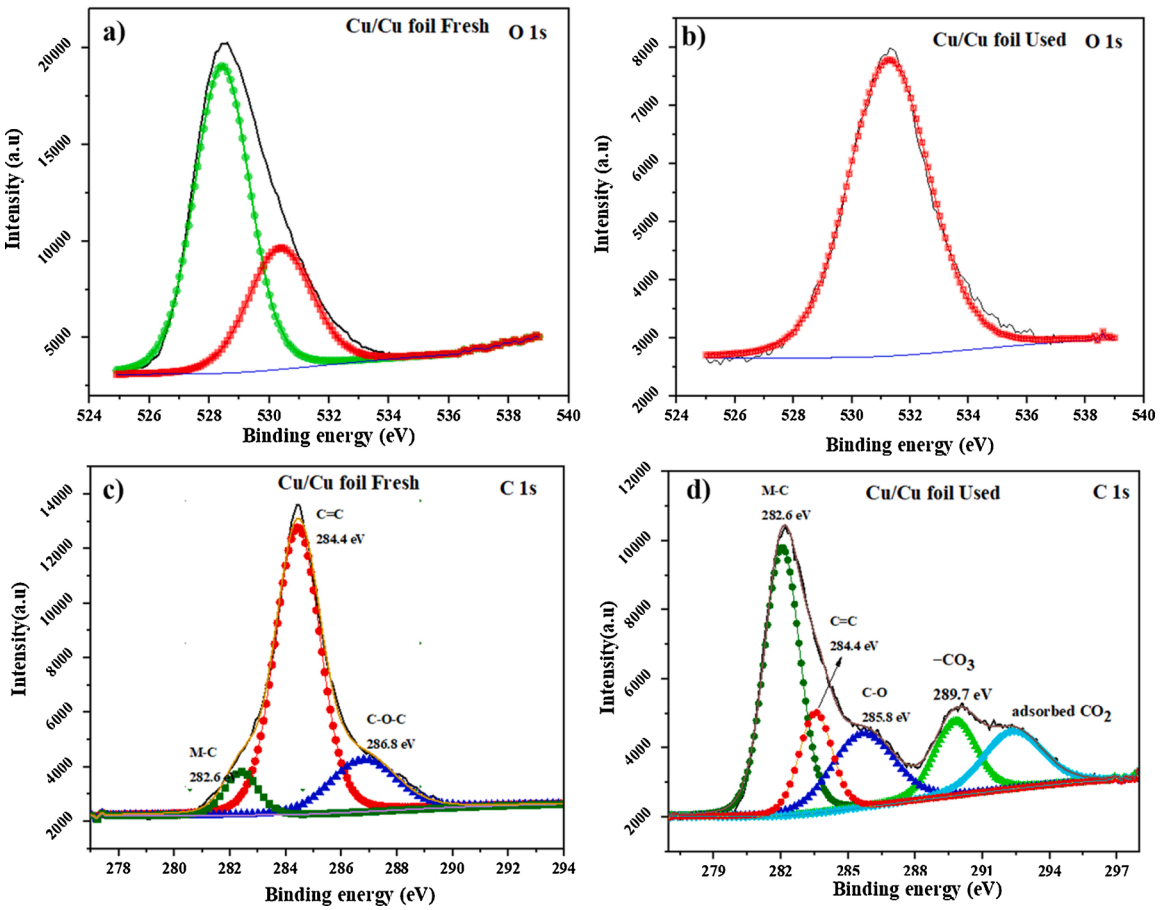

Fig. 8. XPS O 1s and C 1s spectrum of a-c) Cu/Cu fresh b-d) Cu/Cu used catalyst respectively.

corresponding to the —CO_3 species and the other CO_2 molecules/intermediate carbon species in the lattice, respectively. Also there is a noticeable increase in the metal-carbon bond in the catalyst after CO_2 electroreduction. The absorbed CO_2 or its species can atomically interact with the metallic Cu surface to form metal carbide during the reaction that in turn could facilitate the conversion of CO_2 into methanol. XPS O1s spectrum of fresh and used Cu/Z-foil in Fig. S3. The deconvolution profile of O 1s shows the existence of the main broad peak at 531.4 eV (Cu/Zn-foil fresh) and 531.6 eV(Cu/Zn-foil used) indicate the existence of absorbed oxygen on the surface of the catalyst. These results agree with the XRD analysis that the fresh Cu/Zn-foil catalyst contains metallic Cu as a predominant phase without further oxidation. The C 1s spectrum of Cu/Zn-foils represents the existence of C—C,CO and OCO═—— bonds of carbon in the lattice without any significant formation of metal-carbide on the surface or any further formation of carbon species on the surface after the reaction. These results indicates that Cu/Zn-foil shows more stable surface properties that do not undergo any significant changes in the phase of catalyst.

Table S1 shows a comparison of these catalysts with other recently reported promising catalysts. Considering the cost of the raw material (Cu and Zn are non-noble) and the ease of synthesis technique, it is clear that the conversion efficiency reported on Cu/Cu-foil and Cu/Zn-foil for formic acid and methanol are highly significant and promising. These results indicate that the in-situ growth of microparticle over metal foils can prove to be effective for fabricating robust electrodes of converting CO_2 into value-added chemicals. The selectivity, stability and efficiency of the product can be tuned by varying the metallic foils and the surface properties of the deposited particles. Based on the product selectivity and stability, the catalyst shows some promise for large scale applications. Nonetheless, further studies under continuous flow conditions, scale-up analysis and economic feasibility assessments are required to thoroughly evaluate the prospects for industrial applications.

7. Conclusion

In this study, effective and robust electrodes for CO_2 electroreduction were fabricated by in-situ growth of copper microstructures on copper and zinc foils by utilizing the hydrothermal synthesis technique. The electrodes were found to be selective for formic acid, ethyl acetate and methanol generation at the investigated electrode potentials. The high activity and product selectivity were achieved through the structural transformation of Cu particles deposited over Cu-foil and Zn-foil respectively, and provide a practical direction for effective utilization of carbon dioxide to produce value added chemicals. The results indicate that copper supported over metallic foils can be employed for the electrochemical CO_2 reduction to various products, such as formic acid, methanol, ethyl acetate, and changing the metallic foil could prove to be an effective tool for enhancing targeted product selectivity. The electrodes investigated for CO_2 electroreduction were found to be stable, nonetheless some structure changes were observed. Cu/Cu-foils showed the presence of cuboid shape Cu particles with smooth surface and sharp edges after synthesis that were transformed to highly porous cubic microstructures with rough surfaces after the electrocatalytic reaction. In contract, the Cu/Zn-foil was found to be more resistant to structural changes. Cu/Cu-foils showed the highest formic acid efficiency, whereas Cu/Zn-foil was found to be more selective for methanol.

Author statements

Anchu Ashok: Methodology, Investigation, Validation, Writing-

Original draft preparation, **Anand Kumar**: Conceptualization, Methodology, Resources, Writing - Review & Editing, Supervision, Funding acquisition. **Mohammed Ali Saleh Saad**: Resources, Writing - Review & Editing. **Mohammed J Al-Marri**: Resources, Writing- Reviewing and Editing,

Declaration of Competing Interest

The authors declare that they have no known competing financial interests or personal relationships that could have appeared to influence the work reported in this paper.

Acknowledgements

The authors would like to acknowledge the financial assistance from Total Research & Technology Feluy (Grant Number: QUEX-CENG-TRT-17/18). Also, the authors gratefully acknowledge TotalEnergies Research Center Qatar for coordinating this project. The authors are also thankful to Center of Advanced Materials (CAM), Central Laboratory Unit (CLU) and Gas Processing Center (GPC) at Qatar University for providing services related to XRD analysis, electron microscopy and XPS analysis respectively. Open Access funding provided by the Qatar National Library (QNL).

Appendix A. Supplementary data

Supplementary material related to this article can be found, in the online version, at doi:https://doi.org/10.1016/j.jcou.2021.101749.

References

[1] P. Friedlingstein, S. Solomon, G.K. Plattner, R. Knutti, P. Ciais, M.R. Raupach, Long-term climate implications of twenty-first century options for carbon dioxide emission mitigation, Nat. Clim. Change (2011), https://doi.org/10.1038/nclimate1302.

[2] N.P. Gillett, V.K. Arora, K. Zickfeld, S.J. Marshall, W.J. Merryfield, Ongoing climate change following a complete cessation of carbon dioxide emissions, Nat. Geosci. (2011), https://doi.org/10.1038/ngeo1047.

[3] F.D. Meylan, V. Moreau, S. Erkman, CO_2 utilization in the perspective of industrial ecology, an overview, J. CO_2 Util. (2015), https://doi.org/10.1016/j.jcou.2015.05.003.

[4] M. Aresta, A. Dibenedetto, A. Angelini, The changing paradigm in CO_2 utilization, J. CO_2 Util. (2013), https://doi.org/10.1016/j.jcou.2013.08.001.

[5] X. Chen, C. Li, M. Grätzel, R. Kostecki, S.S. Mao, Nanomaterials for renewable energy production and storage, Chem. Soc. Rev. (2012), https://doi.org/10.1039/c2cs35230c.

[6] N.L. Panwar, S.C. Kaushik, S. Kothari, Role of renewable energy sources in environmental protection: a review, Renew. Sustain. Energy Rev. (2011), https://doi.org/10.1016/j.rser.2010.11.037.

[7] R. Nazir, A. Kumar, M. Ali Saleh Saad, S. Ali, Development of CuAg/Cu_2O nanoparticles on carbon nitride surface for methanol oxidation and selective conversion of carbon dioxide into formate, J. Colloid Interface Sci. (2020), https://doi.org/10.1016/j.jcis.2020.06.033.

[8] R. Nazir, A. Khalfani, O. Abdelfattah, A. Kumar, M.A. Saleh Saad, S. Ali, Nanosheet synthesis of mixed Co_3O_4/CuO via combustion method for methanol oxidation and carbon dioxide reduction, Langmuir (2020), https://doi.org/10.1021/acs.langmuir.0c02554.

[9] A. Kumar, A.A.A. Mohammed, M.A.H.S. Saad, M.J. Al-Marri, Effect of nickel on combustion synthesized copper/fumed-SiO_2 catalyst for selective reduction of CO_2 to CO, Int. J. Energy Res. (2021), https://doi.org/10.1002/er.6586.

[10] Q. Li, X. Zhang, X. Zhou, Q. Li, H. Wang, J. Yi, Y. Liu, J. Zhang, Simply and effectively electrodepositing Bi-MWCNT-COOH composite on Cu electrode for efficient electrocatalytic CO_2 reduction to produce HCOOH, J. CO_2 Util. (2020), https://doi.org/10.1016/j.jcou.2019.12.003.

[11] M.E. Günay, L. Türker, N.A. Tapan, Decision tree analysis for efficient CO2 utilization in electrochemical systems, J. CO_2 Util. (2018), https://doi.org/10.1016/j.jcou.2018.09.011.

[12] Y. Hori, Electrochemical CO_2 reduction on metal electrodes, Mod. Asp. Electrochem. (2008), https://doi.org/10.1007/978-0-387-49489-0_3.

[13] C. Costentin, M. Robert, J.M. Savéant, Catalysis of the electrochemical reduction of carbon dioxide, Chem. Soc. Rev. (2013), https://doi.org/10.1039/c2cs35360a.

[14] C. Graves, S.D. Ebbesen, M. Mogensen, K.S. Lackner, Sustainable hydrocarbon fuels by recycling CO_2 and H $_2O$ with renewable or nuclear energy, Renew. Sustain. Energy Rev. (2011), https://doi.org/10.1016/j.rser.2010.07.014.

[15] M. Mikkelsen, M. Jørgensen, F.C. Krebs, The teraton challenge. A review of fixation and transformation of carbon dioxide, Energy Environ. Sci. (2010), https://doi.org/10.1039/b912904a.

[16] K.P. Kuhl, T. Hatsukade, E.R. Cave, D.N. Abram, J. Kibsgaard, T.F. Jaramillo, Electrocatalytic conversion of carbon dioxide to methane and methanol on transition metal surfaces, J. Am. Chem. Soc. (2014), https://doi.org/10.1021/ja505791r.

[17] Y. Wang, D. He, H. Chen, D. Wang, Catalysts in electro-, photo- and photoelectrocatalytic CO_2 reduction reactions, J. Photochem. Photobiol. C Photochem. Rev. (2019), https://doi.org/10.1016/j.jphotochemrev.2019.02.002.

[18] J. Wu, Y. Huang, W. Ye, Y. Li, CO_2 reduction: from the electrochemical to photochemical approach, Adv. Sci. (2017), https://doi.org/10.1002/advs.201700194.

[19] G. Centi, E.A. Quadrelli, S. Perathoner, Catalysis for CO_2 conversion: a key technology for rapid introduction of renewable energy in the value chain of chemical industries, Energy Environ. Sci. (2013), https://doi.org/10.1039/c3ee00056g.

[20] C.W. Li, M.W. Kanan, CO_2 reduction at low overpotential on Cu electrodes resulting from the reduction of thick Cu_2O films, J. Am. Chem. Soc. (2012), https://doi.org/10.1021/ja3010978.

[21] Q. Lu, J. Rosen, F. Jiao, Nanostructured metallic electrocatalysts for carbon dioxide reduction, ChemCatChem (2015), https://doi.org/10.1002/cctc.201402669.

[22] Y.C. Hsieh, S.D. Senanayake, Y. Zhang, W. Xu, D.E. Polyansky, Effect of chloride anions on the synthesis and enhanced catalytic activity of silver nanocoral electrodes for CO_2 electroreduction, ACS Catal. (2015), https://doi.org/10.1021/acscatal.5b01235.

[23] A.M. Appel, J.E. Bercaw, A.B. Bocarsly, H. Dobbek, D.L. Dubois, M. Dupuis, J. G. Ferry, E. Fujita, R. Hille, P.J.A. Kenis, C.A. Kerfeld, R.H. Morris, C.H.F. Peden, A. R. Portis, S.W. Ragsdale, T.B. Rauchfuss, J.N.H. Reek, L.C. Seefeldt, R.K. Thauer, G. L. Waldrop, Frontiers, opportunities, and challenges in biochemical and chemical catalysis of CO_2 fixation, Chem. Rev. (2013), https://doi.org/10.1021/cr300463y.

[24] D. Voiry, H.S. Shin, K.P. Loh, M. Chhowalla, Low-dimensional catalysts for hydrogen evolution and CO_2 reduction, Int. Rev. Chem. (2018), https://doi.org/10.1038/s41570-017-0105.

[25] K.C. Christoforidis, P. Fornasiero, Photocatalysis for hydrogen production and CO_2 reduction: the case of copper-catalysts, ChemCatChem (2019), https://doi.org/10.1002/cctc.201801198.

[26] H. Jiang, Y. Zhao, L. Wang, Y. Kong, F. Li, P. Li, Electrochemical CO_2 reduction to formate on Tin cathode: influence of anode materials, J. CO2 Util. (2018), https://doi.org/10.1016/j.jcou.2018.05.029.

[27] S. Rasul, A. Pugnant, H. Xiang, J.M. Fontmorin, E.H. Yu, Low cost and efficient alloy electrocatalysts for CO_2 reduction to formate, J. CO_2 Util. (2019), https://doi.org/10.1016/j.jcou.2019.03.016.

[28] C.B. Hiragond, H. Kim, J. Lee, S. Sorcar, C. Erkey, S. Il In, Electrochemical CO_2 reduction to CO catalyzed by 2D nanostructures, Catalysts (2020), https://doi.org/10.3390/catal10010098.

[29] M. Morimoto, Y. Takatsuji, R. Yamasaki, H. Hashimoto, I. Nakata, T. Sakakura, T. Haruyama, Electrodeposited Cu-Sn alloy for electrochemical CO_2 reduction to CO/HCOO−, Electrocatalysis (2018) https://doi.org/10.1007/s12678-017-0434-2.

[30] P. Huang, S. Ci, G. Wang, J. Jia, J. Xu, Z. Wen, High-activity Cu nanowires electrocatalysts for CO_2 reduction, J. CO_2 Util. (2017), https://doi.org/10.1016/j.jcou.2017.05.002.

[31] H. Wang, Z. Han, L. Zhang, C. Cui, X. Zhu, X. Liu, J. Han, Q. Ge, Enhanced CO selectivity and stability for electrocatalytic reduction of CO_2 on electrodeposited nanostructured porous Ag electrode, J. CO_2 Util. (2016), https://doi.org/10.1016/j.jcou.2016.04.013.

[32] S. Bashir, S.S. Hossain, S.U. Rahman, S. Ahmed, A. Al-Ahmed, M.M. Hossain, Electrocatalytic reduction of carbon dioxide on SnO_2/MWCNT in aqueous electrolyte solution, J. CO_2 Util. (2016), https://doi.org/10.1016/j.jcou.2016.09.002.

[33] G.O. Larrazábal, A.J. Martín, F. Krumeich, R. Hauert, J. Pérez-Ramírez, Solvothermally-prepared Cu_2O electrocatalysts for CO_2 reduction with tunable selectivity by the introduction of p-Block elements, ChemSusChem (2017), https://doi.org/10.1002/cssc.201601578.

[34] J. Albo, D. Vallejo, G. Beobide, O. Castillo, P. Castaño, A. Irabien, Copper-based metal–organic porous materials for CO_2 electrocatalytic reduction to alcohols, ChemSusChem (2017), https://doi.org/10.1002/cssc.201600693.

[35] K. Ogura, Electrochemical reduction of carbon dioxide to ethylene: mechanistic approach, J. CO2 Util. (2013), https://doi.org/10.1016/J.jcou.2013.03.003.

[36] Y. Hori, H. Konishi, T. Futamura, A. Murata, O. Koga, H. Sakurai, K. Oguma, "Deactivation of copper electrode" in electrochemical reduction of CO_2, Electrochim. Acta (2005), https://doi.org/10.1016/j.electacta.2005.03.015.

[37] Y. Zhao, L. Zheng, D. Jiang, W. Xia, X. Xu, Y. Yamauchi, J. Ge, J. Tang, Nanoengineering metal–organic framework-based materials for use in electrochemical CO_2 reduction reactions, Small (2021), https://doi.org/10.1002/smll.202006590.

[38] M. Naguib, O. Mashtalir, J. Carle, V. Presser, J. Lu, L. Hultman, Y. Gogotsi, M. W. Barsoum, Two-dimensional transition metal carbides, ACS Nano (2012), https://doi.org/10.1021/nn204153h.

[39] N. Li, X. Chen, W.J. Ong, D.R. Macfarlane, X. Zhao, A.K. Cheetham, C. Sun, Understanding of electrochemical mechanisms for CO_2 capture and conversion into hydrocarbon fuels in transition-metal carbides (MXenes), ACS Nano (2017), https://doi.org/10.1021/acsnano.7b03738.

[40] K. Chen, D. Xue, PH-assisted crystallization of Cu_2O: chemical reactions control the evolution from nanowires to polyhedra, CrystEngComm (2012), https://doi.org/10.1039/c2ce26084k.

[41] P. Grosse, D. Gao, F. Scholten, I. Sinev, H. Mistry, B. Roldan Cuenya, Dynamic changes in the structure, chemical state and catalytic selectivity of Cu nanocubes

during CO_2 electroreduction: size and support effects, Angew. Chemie - Int. Ed. (2018), https://doi.org/10.1002/anie.201802083.
[42] L. Zhai, C. Cui, Y. Zhao, X. Zhu, J. Han, H. Wang, Q. Ge, Titania-modified silver electrocatalyst for selective CO_2 reduction to CH_3OH and CH_4 from DFT study, J. Phys. Chem. C (2017), https://doi.org/10.1021/acs.jpcc.7b03314.
[43] Y. Lan, S. Ma, J. Lu, P.J.A. Kenis, Investigation of a Cu(core)/CuO(shell) catalyst for electrochemical reduction of CO_2 in aqueous soultion, Int. J. Electrochem. Sci. (2014).
[44] A. Schizodimou, G. Kyriacou, Acceleration of the reduction of carbon dioxide in the presence of multivalent cations, Electrochim. Acta (2012), https://doi.org/10.1016/j.electacta.2012.05.118.
[45] E. Andrews, M. Ren, F. Wang, Z. Zhang, P. Sprunger, R. Kurtz, J. Flake, Electrochemical reduction of CO_2 at Cu nanocluster / $(10\overline{1}0)$ ZnO electrodes, J. Electrochem. Soc. (2013), https://doi.org/10.1149/2.105311jes.
[46] J. Albo, A. Sáez, J. Solla-Gullón, V. Montiel, A. Irabien, Production of methanol from CO_2 electroreduction at Cu_2O and Cu_2O/ZnO-based electrodes in aqueous solution, Appl. Catal. B Environ. (2015), https://doi.org/10.1016/j.apcatb.2015.04.055.
[47] A. Le Valant, C. Comminges, C. Tisseraud, C. Canaff, L. Pinard, Y. Pouilloux, The Cu-ZnO synergy in methanol synthesis from CO_2, Part 1: origin of active site explained by experimental studies and a sphere contact quantification model on Cu + ZnO mechanical mixtures, J. Catal. (2015), https://doi.org/10.1016/j.jcat.2015.01.021.
[48] Y. Lum, J.W. Ager, Stability of residual oxides in oxide-derived copper catalysts for electrochemical CO_2 reduction investigated with 18 O labeling, Angew. Chemie (2018), https://doi.org/10.1002/ange.201710590.
[49] H. Jung, S.Y. Lee, C.W. Lee, M.K. Cho, D.H. Won, C. Kim, H.S. Oh, B.K. Min, Y. J. Hwang, Electrochemical fragmentation of Cu_2O nanoparticles enhancing selective C-C coupling from CO_2 reduction reaction, J. Am. Chem. Soc. (2019), https://doi.org/10.1021/jacs.8b11237.
[50] S. Ghosh, R. Das, I.H. Chowdhury, P. Bhanja, M.K. Naskar, Rapid template-free synthesis of an air-stable hierarchical copper nanoassembly and its use as a reusable catalyst for 4-nitrophenol reduction, RSC Adv. (2015), https://doi.org/10.1039/c5ra16644f.
[51] Z. Jin, C. Liu, K. Qi, X. Cui, Photo-reduced Cu/CuO nanoclusters on TiO_2 nanotube arrays as highly efficient and reusable catalyst, Sci. Rep. (2017), https://doi.org/10.1038/srep39695.
[52] A. Ashok, A. Kumar, M.A. Matin, F. Tarlochan, Probing the effect of combustion controlled surface alloying in silver and copper towards ORR and OER in alkaline medium, J. Electroanal. Chem. 844 (2019) 66–77, https://doi.org/10.1016/j.jelechem.2019.05.016.
[53] Q. Wang, T. Li, P. Xie, J. Ma, MgO nanolayering of Cu_2O semiconductors enhances photoreactivity: superoxide radicals boost, J. Environ. Chem. Eng. (2017), https://doi.org/10.1016/j.jece.2017.05.023.
[54] Q. Yuan, L. Chen, M. Xiong, J. He, S.L. Luo, C.T. Au, S.F. Yin, $Cu_2O/BiVO_4$ heterostructures: synthesis and application in simultaneous photocatalytic oxidation of organic dyes and reduction of Cr(VI) under visible light, Chem. Eng. J. (2014), https://doi.org/10.1016/j.cej.2014.06.031.
[55] A. Ashok, A. Kumar, R.R. Bhosale, F. Almomani, M.A.H. Saleh Saad, S. Suslov, F. Tarlochan, Influence of fuel ratio on the performance of combustion synthesized bifunctional cobalt oxide catalysts for fuel cell application, Int. J. Hydrogen Energy (2019) 436–445, https://doi.org/10.1016/j.ijhydene.2018.02.111.
[56] A. Ashok, A. Kumar, J. Ponraj, S.A. Mansour, Preparation of mesoporous/microporous $MnCo_2O_4$ and nanocubic $MnCr_2O_4$ using a single step solution combustion synthesis for bifunction oxygen electrocatalysis, J. Electrochem. Soc. 167 (2020), 054507, https://doi.org/10.1149/1945-7111/ab679d.
[57] A. Ashok, A. Kumar, J. Ponraj, S.A. Mansour, F. Tarlochan, Highly active and stable bi-functional $NiCoO_2$ catalyst for oxygen reduction and oxygen evolution reactions in alkaline medium, Int. J. Hydrogen Energy 44 (2019) 16603–16614, https://doi.org/10.1016/j.ijhydene.2019.04.165.
[58] X. Deng, A. Verdaguer, T. Herranz, C. Weis, H. Bluhm, M. Salmeron, Surface chemistry of Cu in the presence of CO_2 and H_2O, Langmuir (2008), https://doi.org/10.1021/la8011052.
[59] M. Favaro, H. Xiao, T. Cheng, W.A. Goddard, E.J. Crumlin, Subsurface oxide plays a critical role in CO2 activation by Cu(111) surfaces to form chemisorbed CO2, the first step in reduction of CO2, Proc. Natl. Acad. Sci. U. S. A. (2017), https://doi.org/10.1073/pnas.1701405114.
[60] A. Ashok, A. Kumar, J. Ponraj, S.A. Mansour, Development of Co/Co9S8 metallic nanowire anchored on N-doped CNTs through the pyrolysis of melamine for overall water splitting, Electrochim. Acta 368 (2021), 137642, https://doi.org/10.1016/j.electacta.2020.137642.
[61] A. Ashok, A. Kumar, J. Ponraj, S.A. Mansour, Synthesis and growth mechanism of bamboo like N-doped CNT/Graphene nanostructure incorporated with hybrid metal nanoparticles for overall water splitting, Carbon N. Y. (2020), https://doi.org/10.1016/j.carbon.2020.08.047.